

THz wave generation by repeated and continuous frequency conversions from pump wave to high-order Stokes waves

Zhongyang Li(李忠洋), Qianze Yan(颜钤泽), Pengxiang Liu(刘鹏翔), Binzhe Jiao(焦彬哲), Gege Zhang(张格格), Zhiliang Chen(陈治良), Pibin Bing(邴丕彬), Sheng Yuan(袁胜), Kai Zhong(钟凯), and Jianquan Yao(姚建铨)
Citation: Chin. Phys. B, 2022, 31 (**7**): 074209. DOI: 10.1088/1674-1056/ac5243
Journal homepage: http://cpb.iphy.ac.cn; http://iopscience.iop.org/cpb

What follows is a list of articles you may be interested in

Noncollinear phase-matching geometries in ultra-broadband quasi-parametric amplification

Ji Wang(王佶), Yanqing Zheng(郑燕青), and Yunlin Chen(陈云琳)
Chin. Phys. B, 2022, 31 (**5**): 054213. DOI: 10.1088/1674-1056/ac3a5b

Creation of multi-frequency terahertz waves by optimized cascaded difference frequency generation

Zhong-Yang Li(李忠洋), Jia Zhao(赵佳), Sheng Yuan(袁胜), Bin-Zhe Jiao(焦彬哲), Pi-Bin Bing(邴丕彬), Hong-Tao Zhang(张红涛), Zhi-Liang Chen(陈治良), Lian Tan(谭联), and Jian-Quan Yao(姚建铨)
Chin. Phys. B, 2022, 31 (**4**): 044205. DOI: 10.1088/1674-1056/ac29b4

High-efficiency terahertz wave generation with multiple frequencies by optimized cascaded difference frequency generation

Zhongyang Li(李忠洋), Binzhe Jiao(焦彬哲), Wenkai Liu(刘文锴), Qingfeng Hu(胡青峰), Gege Zhang(张格格), Qianze Yan(颜钤泽), Pibin Bing(邴丕彬), Fengrui Zhang(张风蕊), Zhan Wang(王湛), and Jianquan Yao(姚建铨)
Chin. Phys. B, 2021, 30 (**4**): 044211. DOI: 10.1088/1674-1056/abe3eb

Theoretical research on terahertz wave generation from planar waveguide by optimized cascaded difference frequency generation

Zhongyang Li(李忠洋), Jia Zhao(赵佳), Wenkai Liu(刘文锴), Qingfeng Hu(胡青峰), Yongjun Li(李永军), Binzhe Jiao(焦彬哲), Pibin Bing(邴丕彬), Hongtao Zhang(张红涛), Lian Tan(谭联), and Jianquan Yao(姚建铨)
Chin. Phys. B, 2021, 30 (**2**): 024209. DOI: 10.1088/1674-1056/abc3b7

Excitation-wavelength-dependent THz wave modulation via external bias electric field

Shi-Jia Feng(冯世嘉), Li-Quan Dong(董立泉), Dan-Ni Ma(马丹妮), Tong Wu(吴同), Yong Tan(谭永), Liang-Liang Zhang(张亮亮), Cun-Lin Zhang(张存林), Yue-Jin Zhao(赵跃进)
Chin. Phys. B, 2020, 29 (**6**): 064210. DOI: 10.1088/1674-1056/ab84d7

THz wave generation by repeated and continuous frequency conversions from pump wave to high-order Stokes waves

Zhongyang Li(李忠洋)[1,†], Qianze Yan(颜钤泽)[1], Pengxiang Liu(刘鹏翔)[2], Binzhe Jiao(焦彬哲)[1], Gege Zhang(张格格)[1], Zhiliang Chen(陈治良)[1], Pibin Bing(邴丕彬)[1], Sheng Yuan(袁胜)[1], Kai Zhong(钟凯)[3], and Jianquan Yao(姚建铨)[3]

[1] *College of Electric Power, North China University of Water Resources and Electric Power, Zhengzhou* 450045, *China*
[2] *Shenyang Institute of Automation, Chinese Academy of Sciences, Shenyang* 110016, *China*
[3] *College of Precision Instrument and Opto-electronics Engineering, Institute of Laser and Opto-electronics, Tianjin University, Tianjin* 300072, *China*

(Received 1 December 2021; revised manuscript received 24 January 2022; accepted manuscript online 7 February 2022)

We propose a novel scheme for THz wave generation by repeated and continuous frequency conversions from pump wave to high-order Stokes waves (HSWs). The repeated frequency conversions are accomplished by oscillations of Stoke waves in resonant cavity (RC) where low-order Stokes waves (LSWs) are converted to high-order Stokes waves again and again. The continuous frequency conversions are accomplished by optimized cascaded difference frequency generation (OCDFG) where the poling periods of the optical crystal are aperiodic leading to the frequency conversions from low-order Stokes waves to high-order Stokes waves uninterruptedly and unidirectionally. Combined with the repeated and continuous frequency conversions, the optical-to-THz energy conversion efficiency (OTECE) exceeds 26% at 300 K and 43% at 100 K with pump intensities of 300 MW/cm^2.

Keywords: THz wave generation, optimized cascaded difference frequency generation, aperiodic periodically poled lithium niobate

PACS: 42.65.Yj, 42.65.Dr, 42.65.Ky **DOI:** 10.1088/1674-1056/ac5243

1. Introduction

In the last two decades, THz science and technology have gained great developments and widely used in biomedicine,[1–3] communications,[4–7] security check,[8,9] THz spectroscopy,[10,11] THz imaging,[12–14] etc. Cascaded difference frequency generation (CDFG) for THz wave generation is a promising method, which can exceed single-photon conversion efficiency.[15–18] However, two problems should be solved for further improving the optical-to-THz energy conversion efficiency (OTECE). Firstly, a large amount of pump photons are not converted to Stokes photons. Two input pump waves and generating Stokes waves pass through optical crystal only once, and the above optical photons are not repeatedly converted into the high-order Stokes photons. Secondly, low-order Stokes photons are difficult to be converted to high-order Stokes photons because phase mismatches are very large especially in high-order cascaded Stokes processes (CSPs).[15,17] Furthermore, THz photons generated by CSPs are consumed by cascaded anti-Stokes processes (CASPs), which further depresses the OTECE.[16] In this work, we introduce a new scheme for THz wave generation with a high OTECE. The scheme solves the above first problem by setting a resonant cavity (RC) for cascaded Stokes waves (CSWs) where low-order Stokes waves (LSWs) are repeatedly converted to high-order Stokes waves (HSWs). The scheme solves the above second problem by optimized cascaded difference frequency generation (OCDFG) where the phase mismatches of CDFG are optimized.

2. Theoretical model

Figure 1(a) is the structural drawing of the proposed scheme. The Bow-tie RC is composed of four cavity mirrors C_1, C_2, C_3 and C_4, which is used in Ref. [19], and the optical crystal is aperiodic periodically poled lithium niobate (APPLN). C_1 and C_2 are two concave mirrors, while C_3 and C_4 are two plane mirrors. C_1 is manufactured with a high transmittance at pump wave (ω_0), signal wave (ω_1), and a high reflectivity at CSWs. C_2 and C_3 set reflecting more than 99.9% for all optical waves. C_2 is specially manufactured with silicon, which transmits THz wave with a small absorption. C_4 has a high transmittance at ω_0, ω_1 and anti-Stokes waves, and has a high reflectivity at CSWs. The specialized fabrication of C_1 and C_4 has been described by Ito.[20] The above cavity mirrors ensure that pump wave, signal wave, THz wave and anti-Stokes waves do not oscillate within the RC, while only the CSWs oscillate within the RC.

In Fig. 1(b), ω_0, ω_1 and THz wave (ω_T) satisfy the first-order phase matching. As long as phase mismatches of CDFG are not large enough, a series of CSWs and THz photons are generated through the CSPs. Simultaneously, CASPs in which

[†]Corresponding author. E-mail: thzwave@163.com

© 2022 Chinese Physical Society and IOP Publishing Ltd

THz photons are consumed and a series of cascaded anti-Stokes waves (CASWs) are generated are stimulated. In this work, ω_m (m is an integer) is CSWs with $m > 1$ and CASWs with $m \leq -1$, respectively. The CSWs oscillate within the cavity, so the frequency conversions among Stokes waves are repeatedly performed. The CASWs are not retained in the resonator, which limits the energy transfer from ω_0 to the CASWs.

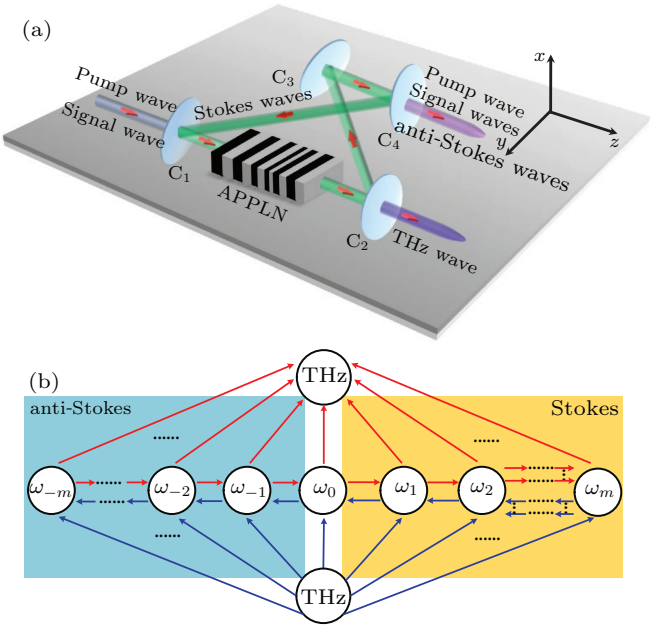


Fig. 1. (a) Schematic diagram describing THz wave generation by OCDFG and the oscillations of Stoke waves in a bow-tie cavity. C_1, C_2, C_3 and C_4 are cavity mirrors. (b) Principle diagram of CSPs and CASPs.

Coupled wave equations of CDFG are reported in Ref. [15]. Different from CDFG, CSWs oscillate within the RC in this work. At each time CSWs interact in APPLN crystal, THz wave is generated and coupled out from RC. Combined the coupled wave equations of CDFG with the theory of optical parametric oscillation, we deduce the coupled wave equations which describes the interactions of CSWs, CASWs, and THz wave, given by

$$\frac{\mathrm{d}E_\mathrm{T}}{\mathrm{d}z} = -\frac{\alpha_\mathrm{T}}{2}E_\mathrm{T} + \sum_{p=1}^{P} R_1^{p-1}R_2^{p-1} \times \left(\mathrm{j}\kappa_\mathrm{T}\sum_{-\infty}^{+\infty} E_m E_{m+1}^{*}\,\mathrm{e}^{\mathrm{j}\Delta k_m z}\right), \quad (1)$$

$$\frac{\mathrm{d}E_m}{\mathrm{d}z} = -\frac{\alpha_m}{2}E_m + \sum_{p=1}^{P} R_1^{p-1}R_2^{p-1} \times \left(\mathrm{j}\kappa_m[E_{m-1}E_\mathrm{T}^{*}\,\mathrm{e}^{\mathrm{j}\Delta k_{m-1}z} + E_{m+1}E_\mathrm{T}\,\mathrm{e}^{-\mathrm{j}\Delta k_m z}]\right), \quad (2)$$

$$\kappa_m = \frac{\Omega_m d_\mathrm{eff}}{cn_m}, \quad (3)$$

$$\kappa_\mathrm{T} = \frac{\Omega_\mathrm{T} d_\mathrm{eff}}{cn_\mathrm{T}}, \quad (4)$$

$$\Delta k_m = k_m - k_{m+1} - k_\mathrm{T} + k_\Lambda, \quad (5)$$

$$I = \frac{1}{2}nc\varepsilon_0|E|^2, \quad (6)$$

$$\eta(z) = \frac{n(\omega_\mathrm{T})|E_\mathrm{T}(\omega_\mathrm{T},z)|^2}{\sum n(\omega_m)|E_m(\omega_m,0)|^2}, \quad (7)$$

where ω and Ω are the frequency and angular frequency, respectively, α is the absorption coefficient, κ is the coupling coefficient, k is the wave vector, n is the refractive index, and the subscripts m and T represent mth-order cascaded wave and ω_T, respectively. E is the electric field strength, Δk represents the phase mismatch, c is the vacuum speed of light, ε_0 represents the vacuum permittivity, I represents the intensity, and Λ represents the poling period of the APPLN. R_1 and R_2 are the reflectance of C_1 and C_2, respectively. P is the oscillation number of Stokes waves, and η represents the OTECE. In Eq. (1), the first item indicates absorption of ω_T and the second item indicates the interaction of cascaded waves to generate ω_T. In Eq. (2), the first item indicates absorption of the cascaded waves, and the second item indicates the generation and consumption of cascaded waves.

3. Calculations

In this work, the pump frequency ω_0 is 291.5 THz, the signal frequency ω_1 is 291 THz, and the generated THz frequency ω_T is 0.5 THz. The calculation of the refractive index of MgO:$LiNbO_3$ crystal in the near-infrared[21] and THz[22] regions is given by the Sellmeier equation. The nonlinear optical coefficient of the MgO:$LiNbO_3$ crystal is 336 pm/V.[15] At 100 K, the absorption coefficient is 0 cm^{-1} for cascaded optical waves and 2.10 cm^{-1} for ω_T.[22] At 300 K, the absorption coefficient is 0 cm^{-1} for cascaded optical waves and 7.20 cm^{-1} for ω_T.[23] The laser induced damage threshold of APPLN with sub-nanosecond is about 10 GW/cm^2.[15] R_1 and R_2 are 0.9999 for CSWs and 0 for ω_0, ω_1 and CASWs. The frequency range of the ω_m is set to 60–500 THz. As shown in Fig. 1(a), the pump and signal waves do not oscillate within the cavity, so the energies of pump and signal waves should be rapidly transferred to Stokes waves firstly, and then further transferred to HSWs. To realize the above anticipation, the APPLN crystal is designed to be two parts, part I and part II. The poling period distributions in part I are given by

$$\Lambda_\mathrm{I} = c \times \left(-n_{0+\frac{M_1\times z}{L}} \times \left(\omega_0 - \omega_\mathrm{T} \times \left(\frac{M_1 \times z}{L}\right)\right) + n_{1+\frac{M_1\times z}{L}} \times \left(\left(\omega_0 - \omega_\mathrm{T} \times \left(\frac{M_1 \times z}{L}\right)\right) - \omega_\mathrm{T}\right) + \omega_\mathrm{T} \times n_\mathrm{T}\right)^{-1}, \quad (8)$$

where $0 < z < L_1$, L_1 is the length of part I, and L is the total crystal length. $M_1 = m - 0$, $m > 1$. Equation (8) leads the Δk_m to be zero step by step from ω_0 to ω_m ($m > 1$), which accelerates the frequency conversions from LSWs to HSWs uninterruptedly

and unidirectionally. The poling period distributions in part II are given by

$$\Lambda_{\mathrm{II}} = c \times \left(-n_{f+\frac{M_2\times(z-L_1)}{L}} \left(\omega_f - \omega_{\mathrm{T}} \times \left(\frac{M_2 \times (z-L_1)}{L} \right) \right) + n_{f+1+\frac{M_2\times(z-L_1)}{L}} \right.$$
$$\left. \times \left(\left(\omega_f - \omega_{\mathrm{T}} \times \left(\frac{M_2 \times (z-L_1)}{L} \right) \right) - \omega_{\mathrm{T}} \right) + \omega_{\mathrm{T}} \times n_{\mathrm{T}} \right)^{-1}, \tag{9}$$

where $L_1 < z < L$. $M_2 = mf$, $m > 1$ and $f < 0$ (f is an integer). ω_f represents the CASWs with the highest intensity generated by part I. Equation (9) leads the Δk_m to be zero step by step from ω_f to ω_m ($m > 1$), which accelerates frequency transformation from the anti-Stokes waves with the highest intensity to HSWs. In Eqs. (8) and (9), M_1 and M_2 which represent the cascading orders from pump frequency or anti-Stokes frequency to high-order Stokes frequency, respectively, are determined by the pump and signal intensities. Figure 2 shows poling period distributions and phase mismatches Δk_m with different pump and signal intensities at 100 K. As shown in Figs. 2(a) and 2(b), when $I_{\mathrm{p}} = I_{\mathrm{s}} = 3$ MW/cm^2, Λ_{I} changes from 237.18 μm to 236.76 μm and Λ_{II} changes from 237.22 μm to 236.77 μm, corresponding to the phase matching of CSPs one order by one order from the first order cascaded Stokes process (CSP) to the 20th order CSP in part I and from the first order cascaded anti-Stokes process (CASP) to the 39th order CSP in part II. As shown in Figs. 2(a) and 2(c), when $I_{\mathrm{p}} = I_{\mathrm{s}} = 3$ MW/cm^2, Λ_{I} changes from 237.18 μm to 236.55 μm and Λ_{II} changes from 237.34 μm to 235.76 μm, corresponding to the phase matching of CSPs one order by one order from the first order CSP to the 40th order CSP in part I and from the third order CASP to the 147th order CSP in part II. As shown in Figs. 2(a) and 2(d), when $I_{\mathrm{p}} = I_{\mathrm{s}} =$ 300 MW/cm^2, Λ_{I} changes from 237.18 μm to 236.36 μm and Λ_{II} changes from 237.49 μm to 234.54 μm, corresponding to the phase matching of CSPs one order by one order from the first order CSP to the 54th order CSP in part I and from the ninth order CASP to the 291th order CSP in part II. Λ_{I} and Λ_{II} are different with different pump and signal intensities. This is because the speed of photon transfer from the mth-order to the $(m+1)$th-order Stokes wave depends on the pump and signal intensities. As the pump and signal intensities increase, the variation of Λ_{I} and Λ_{II} is fast and the crystal length is shortened.

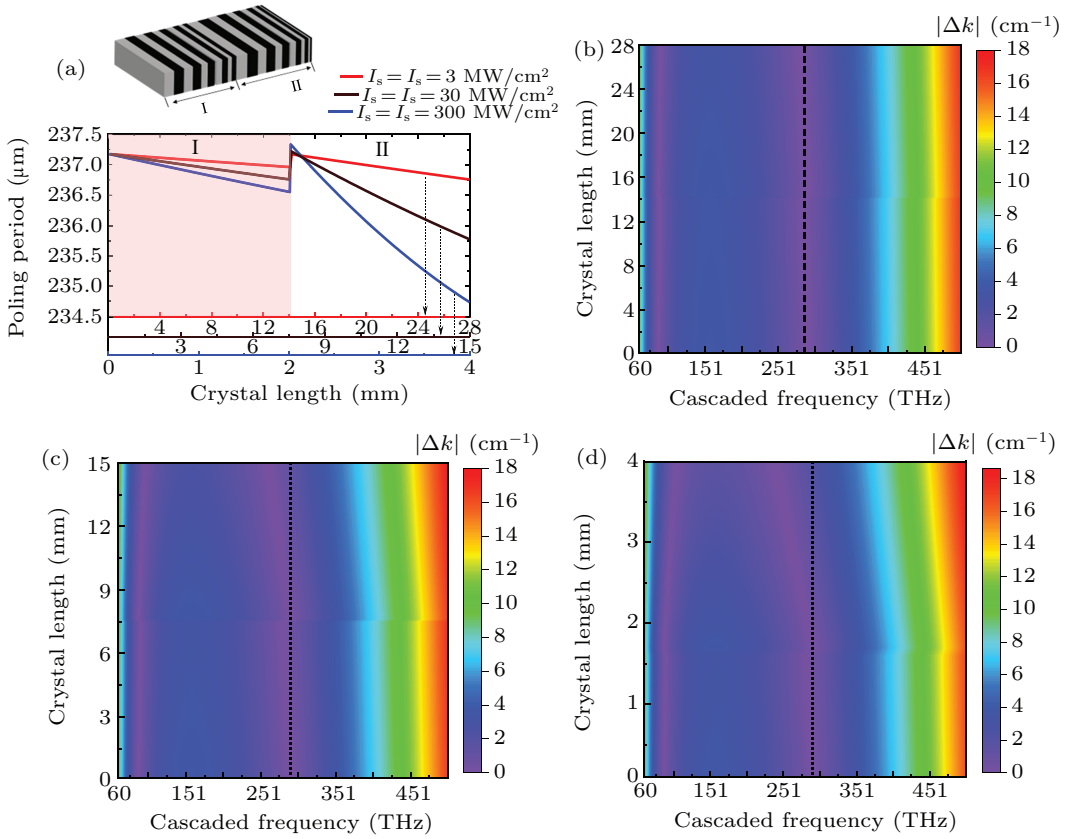


Fig. 2. Poling period distributions and phase mismatches Δk_m with different pump and signal intensities at 100 K. $L = 2 \times L_1$. $I_{\mathrm{p}} = I_{\mathrm{s}} =$ 3 MW/cm^2, $\omega_f = 292$ THz, $M_1 = 20$, $M_2 = 40$; $I_{\mathrm{p}} = I_{\mathrm{s}} = 30$ MW/cm^2, $\omega_f = 293$ THz, $M_1 = 40$, $M_2 = 150$; $I_{\mathrm{p}} = I_{\mathrm{s}} = 300$ MW/cm^2, $\omega_f = 296$ THz, $M_1 = 54$, $M_2 = 300$. (a) Poling period distributions, (b) Δk_m with $I_{\mathrm{p}} = I_{\mathrm{s}} = 3$ MW/cm^2, (c) Δk_m with $I_{\mathrm{p}} = I_{\mathrm{s}} = 30$ MW/cm^2, (d) Δk_m with $I_{\mathrm{p}} = I_{\mathrm{s}} = 300$ MW/cm^2.

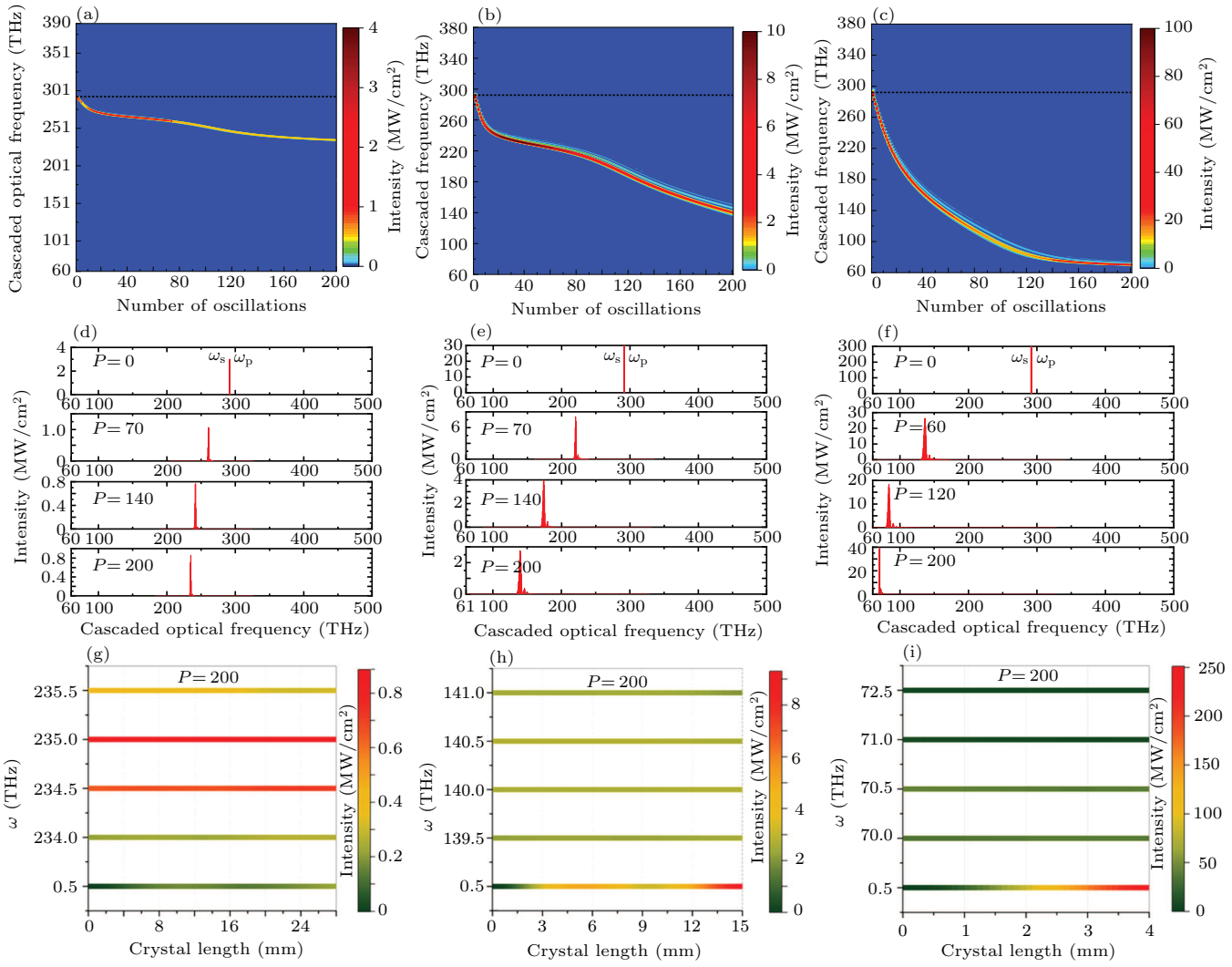


Fig. 3. THz wave intensities and cascaded optical spectra generated by OCDFG in combination with the oscillations of Stoke waves at 100 K. (a) THz wave intensities with $I_p = I_s = 3$ MW/cm^2, (b) THz wave intensities with $I_p = I_s = 3$ MW/cm^2, (c) THz wave intensities with $I_p = I_s = 30$ MW/cm^2, (d) cascaded optical spectral evolution corresponding to (a), (e) cascaded optical spectral evolution corresponding to (b), (f) cascaded optical spectral evolution corresponding to (c), (g) energy distributions of THz wave and cascaded optical waves within the APPLN crystal with $P = 200$ corresponding to (a), (h) energy distributions of THz wave and cascaded optical waves within the APPLN crystal with $P = 200$ corresponding to (b), (i) energy distributions of THz wave and cascaded optical waves within the APPLN crystal with $P = 200$ corresponding to (c).

The intensities of ω_T and the spectral evolution resulting from OCDFG in combination with the oscillations of Stoke waves at 100 K are calculated, as shown in Fig. 3. In Figs. 3(a)–3(c) the anti-Stokes region is above the dashed line and the Stokes region is below the dashed line. The pump and signal photons are converted to high-order Stokes photons one order by one order with the increase of oscillation number P. At each oscillation number P the photons are accumulated to few cascaded optical frequencies. With $I_p = I_s = 3$ MW/cm^2 the energy transfer is slow and the pump photons are not converted to 60 THz, while the energy transfer is rapid and the pump photons are converted to 60 THz at $P = 140$ with $I_p = I_s = 300$ MW/cm^2. From Figs. 3(d)–3(f) we find that cascaded optical spectral evolution is rapid with the oscillation number P. The cascaded optical spectra comprise only a few frequency components. The above results inspire us to generate mid-infrared laser by the novel scheme proposed in this work. Figures 3(g)–3(i) show energy distributions within the APPLN crystal with $P = 200$. The intensity of each cascaded optical wave is constant, while the intensity of ω_T increases rapidly with the crystal length. The maximum ω_T intensities of 0.22 MW/cm^2, 9.89 MW/cm^2, and 260.2 MW/cm^2 are realized when both the pump and signal intensities are 3 MW/cm^2, 30 MW/cm^2 and 300 MW/cm^2, respectively.

Cascaded optical waves intensities generated by OCDFG in combination with the oscillations of Stoke waves at 300 K are calculated, as shown in Fig. 4. The pump and signal photons spread rapidly to the HSWs. Compared with Figs. 3(a)–3(c), the spectral evolution range at 300 K is smaller than that at 100 K with the same inputs. This is because the absorption coefficient of ω_T at 300 K is much larger than that at 100 K, which in turn weakens the OCDFG process. Therefore, the values of M_1 and M_2 at 300 K are smaller than those at 100 K. Figure 5 shows the OTECE corresponding to Figs. 3 and 4, respectively. When both the pump and signal intensities are 3 MW/cm^2, 30 MW/cm^2 and 300 MW/cm^2, the OTECE

reaches 0.12%, 7.65% and 26.57% at 300 K respectively, and reaches 3.73%, 16.49% and 43.37% at 100 K respectively. The higher the pump intensity stimulated, the higher the OTECE obtained. OTECE exceeding 40% at 100 K indicates that ω_T are efficiently generated by repeated and continuous frequency conversions from ω_0 to HSWs in the cavity.

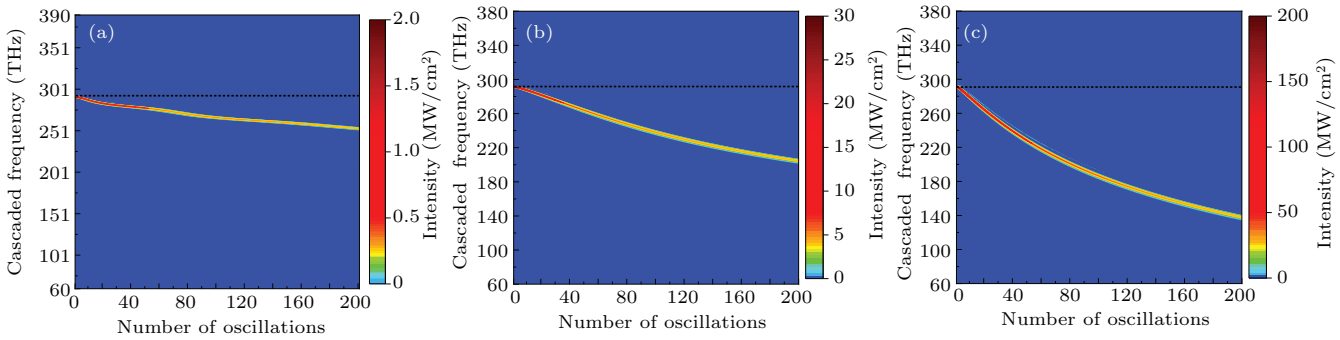


Fig. 4. Cascaded optical spectra generated by OCDFG in combination with the oscillations of Stoke waves at 300 K. (a) $I_p = I_s = 3$ MW/cm^2, $\omega_f = 292$ THz, $M_1 = 20$, $M_2 = 20$ and $L = 50$ mm. (b) $I_p = I_s = 3$ MW/cm^2, $\omega_f = 292$ THz, $M_1 = 20$, $M_2 = 100$ and $L = 8$ mm, (c) $I_p = I_s = 300$ MW/cm^2, $\omega_f = 293$ THz, $M_1 = 28$, $M_2 = 175$ and $L = 3$ mm.

Cascaded optical waves intensities generated by OCDFG without RC at 100 K are calculated, as shown in Fig. 6. The pump and signal photons simultaneously spread to the Stokes and anti-Stokes region. At each pump intensity, a large portion of photons are converted into anti-Stokes region, which consumes THz photons and reduces the OTECE. Moreover, the cascaded Stokes frequency cannot reach 60 THz. Without repeated frequency conversions from ω_0 to HSWs, OCDFG cannot substantially compress the CASPs. As a result, intensity of ω_T generated by OCDFG without RC is significantly suppressed.

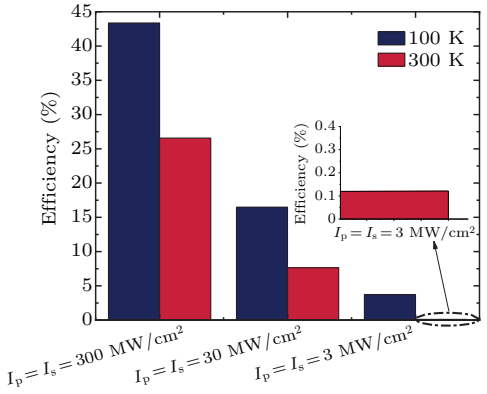


Fig. 5. OTECE at 100 K and 300 K, respectively.

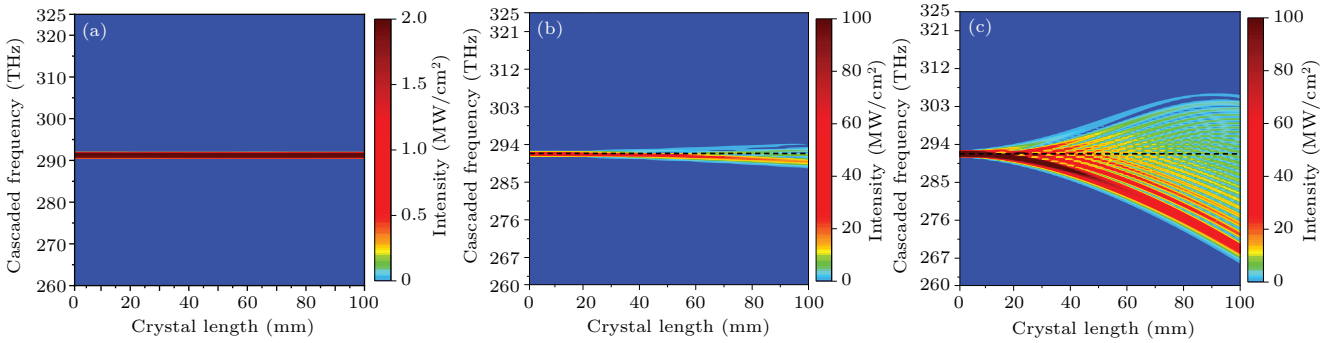


Fig. 6. Cascaded optical spectra generated by OCDFG without RC. The anti-Stokes region is above the dashed line and the Stokes region is below the dashed line. (a) $I_p = I_s = 3$ MW/cm^2, (b) $I_p = I_s = 30$ MW/cm^2, (c) $I_p = I_s = 30$ MW/cm^2.

4. Discussion

Recently,THz wave generations by THz wave parametric oscillator (TPO),[24] difference frequency generation (DFG),[25] and CDFG [18] develop rapidly. For the scheme of TPO, noncollinear phase-matching configuration restricts the interaction volume of mixing waves and depresses the photon conversions from pump wave to THz wave. Jia *et al.* reported a TPO generating THz waves with a $KTiOPO_4$ crystal. When the incident Stokes pulse energy was 36.6 mJ and the pump energy was 580.0 mJ, the obtained maximum THz wave energy was only 17.0 μJ and the quantum efficiency was below 1%.[26] For the scheme of DFG, one pump photon can generate one THz photon at most. Sato *et al.* reported a DFG scheme generating THz waves with a 2D $In_xGa_{1-x}Se$ crystal. The maximum energy of the generated THz wave was 39 pJ and the conversion efficiency was only 1.7×10^{-5} J^{-1}.[27] CDFG is a promising method to generate numerous THz photons from a single pump photon. Ravi *et al.* reported a theoretical work generating THz wave with CDFG under broadband phase matching conditions.[18] The maximum OTECE

of 35% was realized at 10 K. Compared with the Ravi's work, though the absorption coefficients for 0.5 THz at 100 K and 300 K are 8.4 times and 28.8 times higher than that at 10 K respectively, the maximum OTECE of 26.57% at 300 K and 43.37% at 100 K in our work are realized. Compared with the schemes of TPO, DFG and CDFG, the high OTECE in this work is originated from the usage of APPLN in combination with the oscillations of Stoke waves, which can efficiently boost the generation of THz wave by repeated and continuous energy conversions from pump wave to HSWs.

The scheme in this work is practically feasible. Experimental equipment mainly consists of four cavity mirrors, a specially manufactured APPLN crystal and two pump lasers. The fabrication technology of the cavity mirrors has been reported by Ito in 2006. APPLN crystal has been widely utilized for mid-infrared and THz wave generations.[28,29] The Yb:YAG laser with 1030 nm wavelength can be employed as the pump lasers. The intensities of 300 MW/cm^2, 3 MW/cm^2 and 3 MW/cm^2 can be provided by pulsed, quasi-continuous and continuous Yb:YAG lasers respectively, so pulsed, quasi-continuous and continuous THz waves can be generated with the scheme in this work.

5. Conclusions

We introduce a new scheme for high-efficiency ω_{T} generation by OCDFG in combination with the oscillations of Stokes waves. We find that oscillations of Stoke waves rather than other optical waves can repeatedly transfer energies from ω_0 to HSWs, and the modulation of phase mismatches of cascaded optical processes can continuously transfer energies from ω_0 to HSWs. Combined with OCDFG and oscillations of Stokes waves the OTECE exceeds 26% at 300 K and 43.37% at 100 K with the pump intensities of 300 MW/cm^2. The new scheme proposed in this work provides an effective technique to generate pulsed, quasi-continuous or continuous THz waves.

Acknowledgements

Project supported by the National Natural Science Foundation of China (Grant Nos. 61735010, 31671580, and 61601183), Natural Science Foundation of Henan Province, China (Grant No. 162300410190), and Program for Science &Technology Innovation Talents in Universities of Henan Province, China (Grant No. 18HASTIT023).

References

[1] Hong J T, Jun S W, Cha S H, Park J Y, Lee S, Shin G A and Ahn Y H 2018 *Sci. Rep.* **8** 15536
[2] Yan X, Zhang Z, Liang L, Yang M, Wei D, Song X, Zhang H, Lu Y, Liu L, Zhang M, Wang T and Yao J 2020 *Nanoscale* **12** 1719
[3] Yan X, Yang M, Zhang Z, Liang L, Wei D, Wang M, Zhang M, Wang T, Liu L, Xie J and Yao J 2019 *Biosens. Bioelectron.* **126** 485
[4] Nagatsuma T, Ducournau G and Renaud C C 2016 *Nat. Photonics* **10** 371
[5] Yang Y, Yamagami Y, Yu X, Pitchappa P, Webber J, Zhang B, Fujita M, Nagatsuma T and Singh R 2020 *Nat. Photonics* **14** 446
[6] Akyildiz I F, Jornet J M and Han C 2014 *Phys. Commun.* **12** 16
[7] Bai Y, Chen K, Bu T and Zhuang S 2016 *J. Appl. Phys.* **119** 124505
[8] Baxter H W, Worrall A A, Pang J, Chen R and Yang B 2021 *Front. Phys.* **9** 639151
[9] Feng H, An D, Tu H, Bu W, Wang W, Zhang Y, Zhang H, Meng X, Wei W, Gao B and Wu S 2020 *Appl. Phys. B* **126** 143
[10] Neu J, Stone E A, Spies J A, Storch G, Hatano A S, Mercado B Q, Miller S J and Schmuttenmaer C A 2019 *J. Phys. Chem. Lett.* **10** 2624
[11] Bakels S, Gaigeot M P and Rijs A M 2020 *Chem. Rev.* **120** 3233
[12] Guerboukha H, Nallappan K and Skorobogatiy M 2018 *Adv. Opt. Photonics* **10** 843
[13] Wade C G, Šibali N, De Melo N R, Kondo J M, Adams C S and Weatherill K J 2017 *Nat. Photonics* **11** 40
[14] Fan K, Suen J Y, Liu X and Padilla W J 2017 *Optica* **4** 601
[15] Ravi K, Schimpf D N and Kärtner F X 2016 *Opt. Express* **24** 25582
[16] Li Z, Sun X, Li Y, Yuan B, Zhang H, Bing P, Wang Z and Yao J 2020 *Opt. Lasers Eng.* **128** 106035
[17] Ravi K, Hemmer M, Cirmi G, Reichert F, Schimpf D N, Mücke O D and Kärtner F X 2016 *Opt. Lett.* **41** 3806
[18] Ravi K and Kärtner F X 2020 *Laser Photon. Rev.* **14** 2000109
[19] Kiessling J, Sowade R, Breunig I, Buse K and Dierolf V 2009 *Opt. Express* **17** 87
[20] Ikari T, Zhang X, Minamide H and Ito H 2006 *Opt. Express* **14** 1604
[21] Jundt D H 1997 *Opt. Lett.* **22** 1553
[22] Pálfalvi L, Hebling J, Kuhl J, Péter Á and Polgár K 2005 *J. Appl. Phys.* **97** 123505
[23] Fülöp J A, Ollmann Z, Pálfalvi L, Almási G and Hebling J 2011 *Opt. Express* **19** 15090
[24] Kawase K, Shikata J and Ito H 2002 *J. Phys. D* **35** R1
[25] Ding Y J 2014 *JOSA B* **31** 2696
[26] Jia C, Zhang X, Cong Z, Liu Z, Chen X, Qin Z, Zang J, Gao F, Wang P, Jiao Y, Wang W and Zhang S 2020 *Opt. Laser Tech.* **121** 105817
[27] Sato Y, Tang C, Watanabe K, Ohsaki J, Yamamoto T, Tezuka N, Tanabe T and Oyama Y 2020 *Opt. Express* **28** 472
[28] L'huillier J, Torosyan G, Theuer M, Rau C, Avetisyan Y and Beigang R 2007 *Appl. Phys. B* **86** 197
[29] Beddard T, Ebrahimzadeh M, Reid T D and Sibbett W 2000 *Opt. Lett.* **25** 1052